



Battery Wear from Disparate Duty-Cycles: Opportunities for Electric-Drive Vehicle Battery Health Management

Preprint

K. Smith, M. Earleywine, E. Wood,
and A. Pesaran

*Presented at the 2012 American Control Conference
Montreal, Canada
June 27–29, 2012*

NREL is a national laboratory of the U.S. Department of Energy, Office of Energy Efficiency & Renewable Energy, operated by the Alliance for Sustainable Energy, LLC.

Conference Paper
NREL/CP-5400-54698
October 2012

Contract No. DE-AC36-08GO28308

NOTICE

The submitted manuscript has been offered by an employee of the Alliance for Sustainable Energy, LLC (Alliance), a contractor of the US Government under Contract No. DE-AC36-08GO28308. Accordingly, the US Government and Alliance retain a nonexclusive royalty-free license to publish or reproduce the published form of this contribution, or allow others to do so, for US Government purposes.

This report was prepared as an account of work sponsored by an agency of the United States government. Neither the United States government nor any agency thereof, nor any of their employees, makes any warranty, express or implied, or assumes any legal liability or responsibility for the accuracy, completeness, or usefulness of any information, apparatus, product, or process disclosed, or represents that its use would not infringe privately owned rights. Reference herein to any specific commercial product, process, or service by trade name, trademark, manufacturer, or otherwise does not necessarily constitute or imply its endorsement, recommendation, or favoring by the United States government or any agency thereof. The views and opinions of authors expressed herein do not necessarily state or reflect those of the United States government or any agency thereof.

Available electronically at <http://www.osti.gov/bridge>

Available for a processing fee to U.S. Department of Energy and its contractors, in paper, from:

U.S. Department of Energy
Office of Scientific and Technical Information
P.O. Box 62
Oak Ridge, TN 37831-0062
phone: 865.576.8401
fax: 865.576.5728
email: <mailto:reports@adonis.osti.gov>

Available for sale to the public, in paper, from:

U.S. Department of Commerce
National Technical Information Service
5285 Port Royal Road
Springfield, VA 22161
phone: 800.553.6847
fax: 703.605.6900
email: orders@ntis.fedworld.gov
online ordering: <http://www.ntis.gov/help/ordermethods.aspx>

Cover Photos: (left to right) PIX 16416, PIX 17423, PIX 16560, PIX 17613, PIX 17436, PIX 17721



Printed on paper containing at least 50% wastepaper, including 10% post consumer waste.

Battery wear from disparate duty-cycles: Opportunities for electric-drive vehicle battery health management

Kandler Smith, Matthew Earleywine, Eric Wood and Ahmad Pesaran

Abstract—Electric-drive vehicles utilizing lithium-ion batteries experience wholly different degradation patterns from conventional vehicles, depending on geographic ambient conditions and consumer driving and charging patterns. A semi-empirical life-predictive model for the lithium-ion graphite/nickel-cobalt-aluminum chemistry is presented, accounting for physically justified calendar and cycling fade mechanisms. An analysis of battery life for plug-in hybrid electric vehicles considers 782 duty-cycles from travel survey data, superimposed with climate data from multiple geographic locations around the United States. Based on predicted wear distributions, opportunities for extending battery life including modification of battery operating limits, thermal and charge control are discussed.

I. INTRODUCTION

Electric-drive vehicles (EDVs) offer the potential to reduce reliance on fossil fuels; however, the fuel-displacement of EDVs will be elusive until they achieve meaningful market penetration. Batteries are often the most expensive component of the EDV, and further cost reduction is required to make the vehicles more attractive in the marketplace. To compete with conventional vehicles, EDVs and their batteries must achieve a 10 to 15 year life [1]. Cost analyses of light-duty EDVs generally show that periodic battery replacement (e.g., every 5 years) is not warranted and the battery should be designed to last the life of the vehicle [2].

A battery's aging behavior directly impacts what applications and environments to which it is suited, and to what degree the battery must be oversized to achieve desired service life. Conservatism in battery sizing obviously impacts battery cost. Worst-case aging conditions drive the need to oversize batteries, making it important to explore degradation impacts for a range of possible duty-cycles and identify and understand the worst cases. Systems design and control strategies that extend battery life are important to reduce the market cost of EDVs.

From the systems perspective, significant stressors to a lithium (Li)-ion battery include exposure to high temperature, exposure to high charge voltages, calendar age, and depth-of-discharge (DOD) and frequency of charge/

discharge cycles. Various models in the literature, including physics-based [3,4], semi-empirical [5–7], and empirical [8–10], describe the dependence of battery resistance and capacity fade on aging factors. Based on aging datasets for the graphite/nickel-cobalt-aluminum (NCA) Li-ion chemistry, this paper suggests a physically justified semi-empirical model that can be used to interpolate simple laboratory test conditions to arbitrary duty cycles likely to be encountered in real-world environments. The approach is suitable for battery systems engineering and techno-economic analysis of Li-ion batteries.

The paper is organized as follows. Section II introduces the battery life model and regression of model parameters to experimental data. Section III describes vehicle simulation assumptions used to generate 782 single-day battery duty cycles for plug-in hybrid electric vehicles (PHEVs) with 10 and 40 mile (16 and 64 km, respectively) electric range. Section IV presents predicted battery life outcomes across a range of duty-cycle, climate, and charging scenarios and discusses opportunities for life-extending battery systems and controls.

II. BATTERY LIFE MODEL

A. Model description

Ideally, a predictive battery life model should be based on physical mechanisms and should consistently describe degradation under duty-cycles ranging from accelerated calendar and cycling tests to non-accelerated, real-world outcomes. However, non-accelerated aging data are rarely available during the design process.

At the cell terminals, the observable effects of degradation are an increase in resistance and reduction in capacity. These two effects can be correlated with power and energy loss that cause battery end-of-life in an application. Mechanisms for resistance growth include loss of electrical conduction paths in the electrode, fracture or isolation of active material, growth of film layers at the electrode surface, and degradation of electrolyte. Mechanisms for capacity loss include fracture, isolation, or chemical degradation of active material and loss of cycleable Li from the system as a product of side reactions.

Under storage or calendar-aging conditions, the present model assumes the dominant fade mechanism to be growth of a resistive layer at the solid/electrolyte interface (SEI). As the layer grows, it consumes cycleable Li from the system, reducing capacity. Consistent with a diffusion-limited growth process [3], the model assumes SEI-resistance growth and

This work was supported by the U.S. Department of Energy, Office of Energy Efficiency and Renewable Energy, Vehicle Technologies Energy Storage Program.

Kandler Smith is with the National Renewable Energy Laboratory (NREL), Golden, CO 80401 USA (303-275-4423; e-mail: kandler.smith@nrel.gov). Matthew Earleywine, Eric Wood, and Ahmad Pesaran are also with NREL (e-mail: matthew.earleywine@nrel.gov, eric.wood@nrel.gov, ahmad.pesaran.nrel.gov).

Li-capacity loss are proportional to the square-root of time, respectively $R_{SEI} \sim a_1 t^{1/2}$ and $Q_{Li} \sim b_1 t^{1/2}$.

Under cycling-intense conditions, the model assumes degradation is primarily due to structural degradation of the electrode matrix and active sites. Resistance growth and capacity fade are assumed to be proportional to the number of cycles, $R_{sites} \sim a_2 N$ and $Q_{sites} \sim c_1 N$, respectively.

Cell resistance growth due to calendar- and cycling-driven mechanisms are assumed to be additive,

$$R = a_0 + a_1 t^{1/2} + a_2 N. \quad (1)$$

Cell capacity is assumed to be controlled by either loss of cycleable Li or loss of active sites,

$$Q = \min(Q_{Li}, Q_{sites}) \quad (2)$$

where

$$Q_{Li} = b_0 + b_1 t^{1/2} \quad (3)$$

$$Q_{sites} = c_0 + c_1 N \quad (4)$$

Equations (2-4) are a simplification of observations from experimental data [11]. Note that electrode site capacity, Q_{sites} , in (2) may be expanded to include separate terms for negative electrode sites and positive sites; however, it is common for one electrode to limit active-site capacity.

The parameters in (1), (3), and (4) can be regressed to match resistance and capacity fade data for any individual aging condition. To capture life dependence on duty-cycle, acceleration functions are needed to describe dependence of rate coefficients a_1 , a_2 , b_1 , and c_1 on appropriate duty-cycle stress factors. Based on data described in the next section, stress factors are chosen as temperature, open-circuit voltage [related to the state of charge (SOC)], and DOD of each cycle. Due to the limited amount of aging data available, mechanical stress and fracture due to high-rate discharge/charge cycling are neglected in the present model. However, accelerated chemical stress due to elevated temperature under high-rate cycling is captured.

For a generic rate coefficient θ representing a_1 , a_2 , b_1 , and c_1 , the present model assumes Arrhenius dependence on temperature $T(t)$,

$$\theta_T = \exp\left[\frac{-E_a}{R_{ug}}\left(\frac{1}{T(t)} - \frac{1}{T_{ref}}\right)\right], \quad (5)$$

Tafel dependence on open-circuit voltage $V_{oc}(t)$,

$$\theta_V = \exp\left[\frac{\alpha F}{R_{ug}}\left(\frac{V_{oc}(t)}{T(t)} - \frac{V_{oc,ref}}{T_{ref}}\right)\right], \quad (6)$$

and Wöhler dependence [12] on individual swings in DOD ΔDOD_i ,

$$\theta_{\Delta DOD} = \left(\frac{\Delta DOD_i}{\Delta DOD_{ref}}\right)^\beta. \quad (7)$$

The combination of individual stress factors is assumed to be multiplicative,

$$\theta = \theta_{ref} \Pi \theta_k \quad (8)$$

In the above, E_a , α , β , and θ_{ref} are fitting parameters; R_{ug} is the universal gas constant; F is the Faraday constant; and $T_{ref} = 298.15\text{K}$, $V_{oc,ref} = 3.6\text{V}$, and $\Delta DOD_{ref} = 1$ are arbitrary constants included for convenience of comparing θ_{ref} to standard aging conditions.

B. Regression of model parameters

The life model is fit to multiple aging datasets for the graphite/NCA Li-ion chemistry, providing a general representation of aging for that chemistry. The parameters for temperature, voltage, and DOD acceleration are fit to aerospace cell data from the literature, as summarized in Table 1. Final rate constants are adjusted to match cells specifically designed for EDV application.

Table 1. Composite dataset used to populate graphite/NCA life model.

	Test	Source	Temperature	End-of-Chg. or Storage Voltage	Depth-of-Discharge	Cycles/day
Fitted Data	Resistance	Broussely (Saft), 2007	20,40,60°C	3.6,4.1V	Storage	0
	Growth	Hall (Boeing), 2006	20°C	3.9,4.0,4.1V	20,40,60,80%	1,4
	Capacity Fade	Smart (NASA), 2009	10,23,40,55°C	3.6V	Storage	0
		Broussely (Saft), 2001	20°C	3.6,4.1V	Storage	0
Validation Cases	HEV combined cycling + calendar	Belt (Idaho Nat. Lab.), 2008	30,45,53°C	3.6V	1.5%	95,290,500
			25°C	4.0V	75%	4
	PHEV accelerated cycling	Gaillac (S. Calif. Edison), 2009	25°C	4.0V	75%	4

Figure 1 shows resistance growth with storage at three temperatures and two SOCs [13]. Figure 1a compares models, Eq. (1) with $N=0$, regressed to each individual test condition. Figure 1b shows the resistance growth rate a_1 for each tested condition. An Arrhenius-Tafel model, i.e., the product of (5) and (6) in (8), describes the dependence of resistance growth rate for all storage conditions.

Figure 2 shows resistance growth with cycling for three end-of-charge voltages and six DODs at a single temperature [14]. The set of aging tests, designed to mimic a geosynchronous orbit satellite application, were run in both an accelerated (4 cycles/day) and non-accelerated (1 cycle/day) manner. Simultaneous nonlinear least-squares regression of all eight cycling conditions, accounting for the ΔDOD and $V_{oc}(t)$ of each profile, gives dependence of resistance growth rate a_2 , corrected to a reference voltage as shown in Fig. 2a. The Tafel-Wöhler model, i.e., the product of (6) and (7) in (8), reproduces measured resistance trajectories for the entire dataset.

Under the same geosynchronous satellite cycling conditions, Hall *et al.* [14] observed an apparent mechanism shift in capacity fade rates between the accelerated and non-accelerated cycling conditions. The authors demonstrated significantly different cycle-life projections depending upon whether the accelerated or the non-accelerated dataset was used to make the projection. The present capacity fade model (2) attributes the mechanism shift to a transition between capacity fade dominated by Li loss (3) and capacity fade dominated by active-site loss (4). Figure 3 shows capacity fade for the range of cycling conditions described by the two-mechanism model. Again, the fitting procedure accounts for the specific ΔDOD and $V_{oc}(t)$ of each tested condition.

Outside of the satellite industry, it is exceedingly rare, due to the obvious extra time and cost associated with the non-accelerated tests, that cycling tests are run in both an accelerated and non-accelerated manner. Yet the possible mechanism shift between the two test methods [14] has important implications for extrapolation of accelerated test results. Additional research is needed to clarify relationships between calendar- and cycling-controlled capacity fade mechanisms in order to provide more robust prediction of capacity fade forward in time.

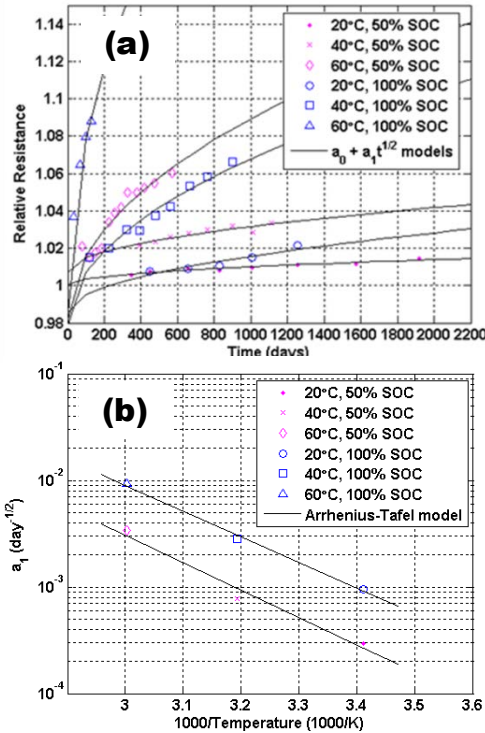


Fig. 1. Resistance growth under storage at multiple temperatures and SOC [13]. (a) Each tested condition separately fit with models of the form $a_0 + a_1 t^{1/2}$. (b) Variation of parameter a_1 captured by Arrhenius-Tafel model describing the entire dataset.

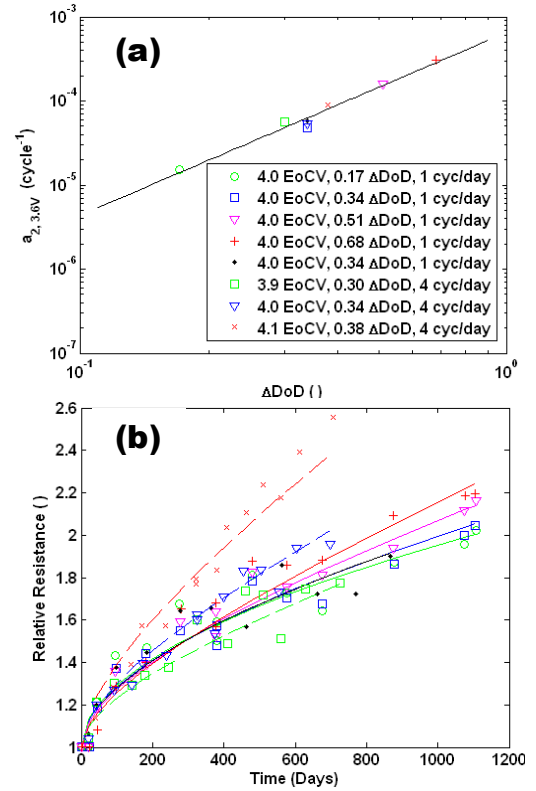


Fig. 2. Resistance growth at 20°C under multiple cycling conditions [14] fits with Eq. (1): (a) Variation of parameter a_2 captured by Tafel-Wöhler model. (b) Comparison of final model with entire dataset.

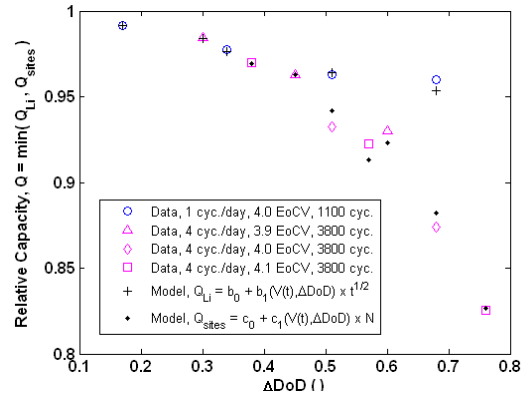


Fig. 3. Capacity fade [14] at 20°C under multiple cycling conditions fits with Eqs. (2-4).

III. BATTERY DUTY-CYCLES

A. Vehicle assumptions

The analysis considers two midsize PHEVs with batteries providing nominal 10- and 40-mile all-electric range for a urban dynamometer driving schedule (UDDS) driving cycle. Following a charge depletion (CD) mode supported primarily by the battery, vehicle operation switches to a charge sustaining (CS) mode supported by a gasoline fueled internal combustion engine. Vehicle model parameters are given in Table 2.

Table 2. Vehicle model inputs

		PHEV10	PHEV40
Vehicle	All-electric range, km	16.7	67
	Total vehicle mass, kg	1714	1830
	Electric motor power, kW	40	43
	IC engine power, kW	77	80
Battery Electrical¹	Useable power, kW	44	48
	Useable energy, kWh	2.67	11.48
	Maximum SOC	80%	90%
	Minimum SOC at BOL	30%	30%
	Minimum SOC at EOL	13%	10%
	Excess energy at BOL	100%	67%
Battery Thermal	Excess power at BOL, 10% SOC	43%	43%
	Heat transfer area - cells-to-coolant, m ²	1	3
	Heat transfer area - pack-to-ambient, m ²	1.2	2.9
	Heat transfer coeff. - pack-to-ambient, W/m ² K	2	2

1. EOL condition = 75% remaining capacity

B. Vehicle drive-cycle distribution

Light-duty vehicle drive-cycles are taken from a Texas Department of Transportation travel survey in San Antonio and Austin [17]. A subset of that survey recorded speed versus time data for 782 individual light duty vehicles, each over a 24-hour period. Previous NREL analysis estimated PHEV fuel economy for all 782 drive cycles [18].

Two different charging scenarios are considered, (i) nightly charging, in which the driver charges the vehicle immediately following the final driving trip of the day, and (ii) opportunity charging, in which the driver charges the vehicle at each stop lasting longer than 2 minutes. Both charging scenarios assume a 1.6 kW rate.

Battery power profiles from vehicle simulations serve as input to the battery life model. For prediction of battery life, it is necessary to assume how often each single-day trip occurs. The present analysis considers each drive-cycle individually and assumes 1 day of rest for each 6.8 days of driving. This frequency of trips is chosen so that the average travel distance from the Texas survey, 38.9 miles/day (62.6 km/day) compares to the U.S. national average for annual distance traveled, 12,375 miles/year (19,916 km/year) [19].

C. Geographic temperature distribution

Recent NREL analysis [20] used hybrid electric vehicle registration data from the Polk Company for the top 100 cities in the United States as a proxy for likely PHEV sales distributions within the United States. This paper considers the hottest and median climates of those 100 cities in terms of typical battery wear, respectively, Phoenix, Arizona, and Baltimore, Maryland. Using the method described in [21], those respective geographic locations are represented using equivalent battery aging temperatures of 28°C and 16°C to reduce the complexity of hour-by-hour temperature variation. The present analysis thus does not account for worst-case start-up and operability limits on the battery, but rather compares typical battery degradation rates that may be expected for PHEVs operating in hot and median U.S. climates.

D. Battery thermal model

Two possible battery thermal management (BTM) configurations are considered with a simple thermal model. The “Limited BTM” case assumes the battery is cooled using forced air ($h = 15 \text{ W/m}^2\text{K}$) taken from outside ambient. The “Aggressive BTM” case assumes the battery is cooled with a chilled liquid ($h = 80 \text{ W/m}^2\text{K}$) supplied to the battery cell surfaces at 20°C. Battery heat generation rates are taken from the vehicle simulation model. The cooling system is active during both driving and charging.

IV. RESULTS

The matrix of scenarios considered in the present battery life analysis is:

- PHEV10 and PHEV40 midsize sedans,
- hot and median geographic regions,
- nightly and opportunity charge scenarios, and
- isothermal, limited and aggressive thermal management scenarios.

Figure 4 shows statistics of remaining capacity after 8 years of repeated battery cycling under each of the 782 driving cycles. Under the artificially imposed isothermal condition, the hot climate case (28°C) shows 50% greater capacity loss compared to the median climate (10°C). Differences between hot and median climates narrow slightly when considering more realistic battery temperature evolution with time under limited and aggressive BTM scenarios. The limited BTM system assumes that forced ambient air cools the battery, resulting in temperature rise above ambient and a shorter battery life relative to the isothermal case. The aggressive BTM system assumes that 20°C chilled fluid cools the

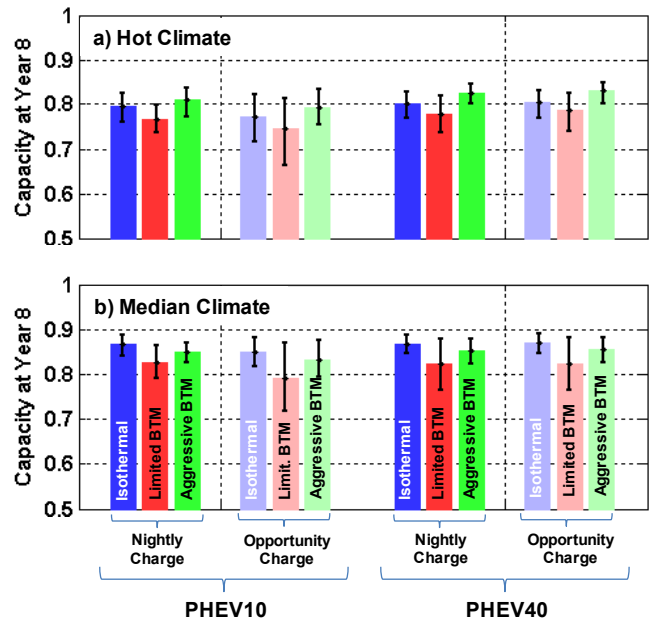


Figure 4. Remaining capacity at the end of 8 years for various BTM and charging scenarios. Colored bars show average result for all 782 drive cycles. Error bars show result for 5th and 95th percentile drive cycles.

battery, which in the hot climate results in a slightly longer life relative to the isothermal case. In Fig. 4, error bars denoting degradation for 5th and 95th percentile drive cycles show that limited BTM causes larger deviations in battery life compared to aggressive BTM—an undesirable outcome.

In Fig. 4, the PHEV10 and PHEV40 generally experience similar degradation trends. The impact of charging behavior is an exception. The PHEV10 battery suffers more degradation from opportunity charging than the PHEV40. This is because the PHEV10 battery's useable CD energy content is cycled deeper and more often than the PHEV40's battery for the same driving trip distance. In general, worst-case battery life results from frequent recharging scenarios. In addition to increased cycling of the batteries, opportunity charging is accompanied by almost continuous heat generation throughout the day, which is not conducive to limited BTM system designs. Fast charge capability, not considered in the present work, can be expected to result in even more stringent thermal requirements on the BTM system and cycle-life requirements on the battery cells.

To help explain degradation rate differences resulting from the various duty-cycles, Fig. 5 presents remaining capacity at year 8 for the PHEV10 nightly-charge aggressive-cooling case. Outcomes are plotted versus the three stress factors considered in the life model. For visualization purposes, Fig. 5 neglects interactions between temperature, SOC, and cycling-rate-per-day and presents the three stress factors as an effective temperature,

$$T_{eff} = \frac{(-E_a + \alpha F V_{oc,avg})/R_{ug}}{\ln\left\{\frac{1}{t_{day}} \int_0^{t_{day}} \exp[-E_a + \alpha F V_{oc}(t)]/R_{ug} T(t) dt\right\}}, \quad (9)$$

effective open-circuit voltage,

$$V_{oc,eff} = \frac{\ln\left\{\frac{1}{t_{day}} \int_0^{t_{day}} \exp[\alpha F V_{oc}(t)]/R_{ug} T(t) dt\right\}}{\alpha F/R_{ug} T_{avg}}, \quad (10)$$

which is expressed in Fig. 5 as effective SOC using the static functional relationship, $SOC_{eff} = f(V_{oc,eff})$, and effective number of cycles-per-day,

$$\dot{N}_{eff} = \frac{1}{t_{day}} \left[\sum_i N_i \left(\frac{\Delta DOD_i}{\Delta DOD_{ref}} \right)^\beta \right]^{1/\beta}. \quad (11)$$

With $\Delta DOD_{ref} = 100\%$, Eq. (11) aggregates all individual microcycles into a single statistic of equivalent number of 100% DOD cycles/day.

In Fig. 5, the population with the shortest life appears as the dark blue cluster. This group has high cycles-per-day (corresponding to daily trip distances greater than 10 miles), yet spends significant time at high SOC (corresponding to one or several closely grouped trips-per-day that are

immediately followed by battery recharge). For this PHEV10 scenario, the populations with the longest life result either from cycles with low daily mileage (front-left corner of Fig. 5) or those with high daily mileage (back-right portion of Fig. 5). Unique to this nightly charge scenario, the high-mileage drive-cycles spend significant time in CS mode at low SOCs, conducive to long battery life.

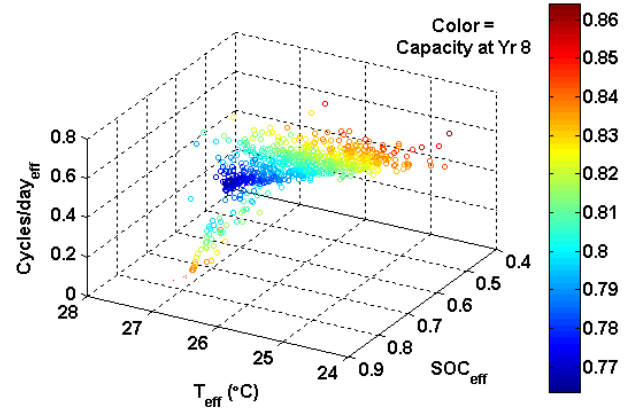


Figure 5. Remaining capacity at end of 8 years for PHEV10 nightly-charge aggressive-cooling hot-climate scenario. For this charging scenario, the effective cycles-per-day is capped near 0.5, corresponding to the PHEV10 useable CD limit of 50% ΔDOD . Worst-case degradation occurs for batteries that use all of their available CD energy range, yet still spend much of their life at high SOCs.

Figure 6 shows the same PHEV10 hot-climate aggressive cooling case, but under an opportunity charge scenario. With frequent charging between trips, the same high mileage drivers with good battery life in Fig. 5 suddenly move to the population with highest capacity fade due to frequent deep cycling of the battery. The worst case remaining capacity at 8 years drops from 77% (Fig. 5) to 65% (Fig. 6) when charging behavior changes from nightly to opportunity. The worst-case drive cycle in Fig. 6 experiences the equivalent cycling stress of one full discharge event per day.

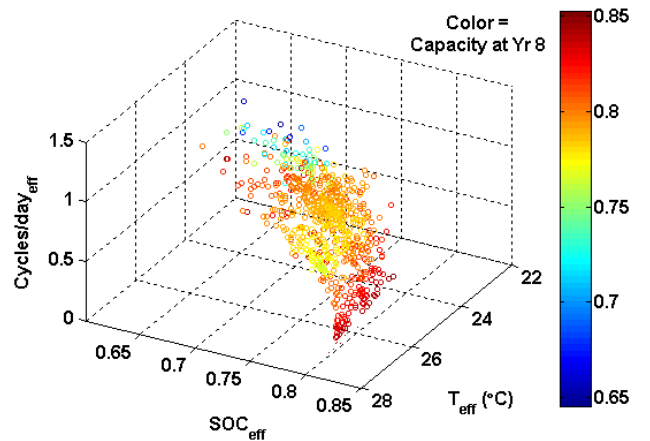


Figure 6. Remaining capacity at end of 8 years for PHEV10 opportunity-charge aggressive-cooling hot-climate scenario. Unlike the nightly-charge scenario (Fig. 5), multiple charging events mean that effective cycles-per-day is not capped near the PHEV10 useable CD limit of 50% ΔDOD .

Even though high-mileage driving and frequent charging can cause short PHEV10 battery life, the high utilization of all-electric CD mode can decrease vehicle operating costs due to the cheaper cost of electricity relative to gasoline. Depending on whether battery replacement cost is prorated for the remaining years of life, the relative low expense of all-electric operation can make battery replacement economically feasible for some high-mileage drivers.

Unique to BTM systems that utilize chilled coolant in hot climates, in Fig. 6, the drive cycles with high cycles per day have the lowest temperature. Not shown is the limited BTM case, which shows the opposite: high battery temperatures that correlate with high mileage. Compared to the aggressive BTM scenario shown, the limited cooling BTM scenario holds generally similar degradation trends with respect to effective cycles-per-day and SOC, albeit with overall shorter life, and higher and more variable temperature.

Compared to the PHEV10 battery, the larger PHEV40 battery's life is less dependent on charging behavior. Figure 7 displays life outcomes as a difference between opportunity and nightly charge cases for each individual drive cycle. The PHEV40 change in 8-year-capacity ranges from 4% gain to 3% loss in capacity. Overall, a slight majority of the PHEV40 population achieves longer life with opportunity charging behavior due to the shallower CD cycles that occur as a result of more frequent charging. In contrast, a significant portion of the PHEV10 population will experience a shorter life from opportunity charging with as much as 20% additional capacity fade at year 8. In Fig. 7, the purple "x" symbol demarks PHEV10 drive-cycles with annual mileage greater than 12,500 miles/year. Those high-mileage drive-cycles account for many of the worst life outcomes for the PHEV10 vehicle when it is opportunity-charged.

While a warranty may protect the manufacturer from bearing the cost of battery replacement for customers with high-mileage frequent-charging behavior, it is still desirable, if possible, to influence battery duty-cycle to extend calendar life. Possible methods include lowering average daily temperature, lowering daily maximum DOD, reducing the cycles-per-day, and reducing the average daily SOC. Figure 8 shows that reducing the effective number of cycles-per-day by 0.15 (from 1 to 0.85 100% DOD-equivalent cycles) can improve year 8 capacity by some 10%. Decreasing effective SOC by 5% can improve year 8 capacity on the order of 1%. Possible methods to accomplish this are by lowering the maximum SOC or end-of-charge voltage for drivers with frequent charging behavior to limit CD mode energy throughput. It may also be possible to reduce allowable power limits for CS and CD mode operation to effect slight reductions in effective cycles-per-day.

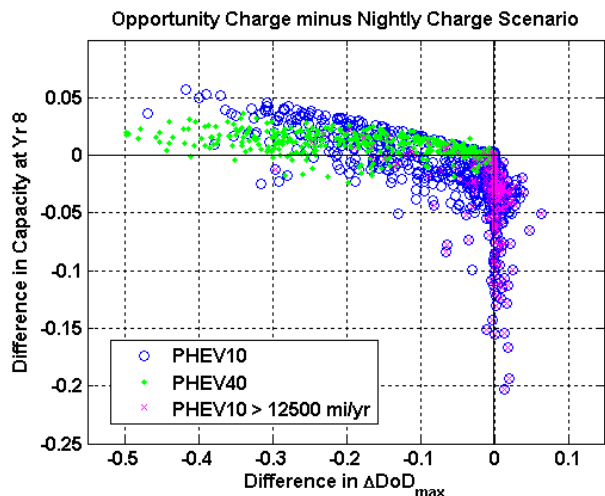


Figure 7. Difference in life outcomes for opportunity charging behavior versus nightly charging behavior (aggressive-cooling, hot-climate scenario). PHEV40 drive cycles generally benefit from opportunity charging, owing to shallower cycling. Many PHEV10 drive cycles, particularly those with high annual mileage, experience increased battery fade from opportunity charging due to increase CD energy throughput.

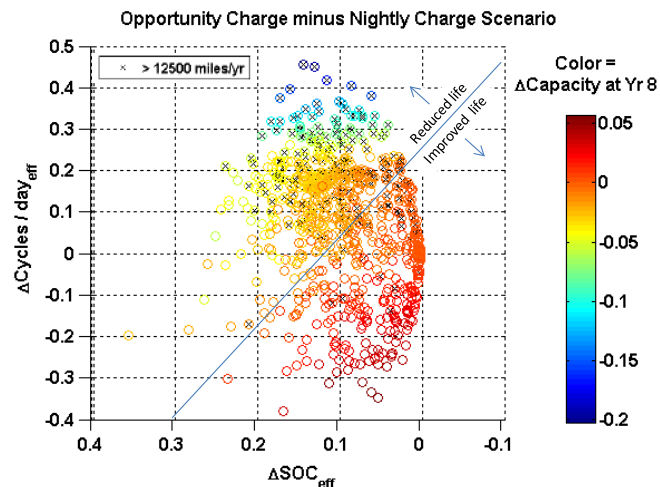


Figure 8. Differences in PHEV10 life outcomes for opportunity charging versus nightly charging behavior (aggressive-cooling, hot-climate scenario). An approximate line is drawn at the transition between reduced life and improved life, resulting from frequent charging.

V. CONCLUSION

Thermal management system design is shown to be effective in extending battery life, particularly for the most severe discharging and frequent recharging duty-cycles. Aggressive thermal management reduces the standard deviation in life outcomes for a given range of duty-cycles. Use of a refrigerated or chilled-fluid cooling system extends calendar life in hot climates. For batteries experiencing high-average temperature, life-extending controls might reduce allowable power limits at high temperature, gradually reduce temperature control set-points, or otherwise increase cooling system use at the expense of additional parasitic loss.

Across a range of possible PHEV duty-cycles, worst-case battery life results from frequent recharging scenarios, particularly for the PHEV10 as its small battery is

discharged through the entire useable CD energy range for 82% of the population of drive cycles. Frequent charging scenarios will result in the highest cycle-life requirements for battery cells, and highest cooling requirements for battery thermal management systems.

Compared to CD mode of PHEV operation, battery wear induced during CS mode is small. Calibration parameters for CD mode are critical to achieving long battery life. With some impact on useable all-electric range, life-extending controls might reduce maximum SOC, reduce allowable DOD in CD and CS modes, and reduce power limits on charge and discharge, particularly important at temperature extremes and high SOCs. A slight reduction in all-electric range performance may be desirable to increase battery calendar life for consumers who charge frequently. Provided battery wear can be managed, frequent charging behavior should generally be encouraged as increased all-electric operation reduces operating costs and petroleum usage.

Any control-induced reduction in all-electric range must take into account emissions regulations that can drive warranty requirements for PHEV batteries. Life-extending control should seek to find the optimum balance of total lifetime emissions and vehicle cost of ownership, which accounts for battery life that meets warranty and emissions regulations constraints and guarantees vehicle performance acceptable to the consumer.

VI. ACKNOWLEDGMENT

The authors gratefully acknowledge funding and support from the U.S. Department of Energy Office of Vehicle Technologies Energy Storage program managers, David Howell and Brian Cunningham, and for helpful discussions from Loïc Gaillac, John Hall, Naum Pinsky, and Marshall Smart.

VII. REFERENCES

- [1] U.S. Council for Automotive Research, "USABC Plug-in HEV Battery Goals," http://www.uscar.org/guest/article_view.php?articles_id=85.
- [2] E. Wood, M. Alexander, T.H. Bradley, "Investigation of battery end-of-life conditions for plug-in hybrid electric vehicles," *J. Power Sources* 196 (2011) 5147-5154.
- [3] H.J. Ploehn, P. Ramadass, R.E. White, "Solvent diffusion model for aging of lithium-ion battery cells," *J. Electrochemical Society*, 151 (3), 2004, A456-A462.
- [4] M. Safari, M. Morcrette, A. Teyssot, C. Delacourt, "A Multimodal physics-based aging model for life prediction of Li-ion batteries" *J. Electrochem. Soc.*, 156(3), A145-A153 (2009)
- [5] R. Spotnitz, "Simulation of capacity fade in lithium-ion batteries," *J. Power Sources*, 113(1), 2003, 72-80.
- [6] K. Smith, T. Markel, A. Pesaran, "PHEV battery trade-off study and standby thermal control," 26th Int. Battery Seminar & Exhibit, Fort Lauderdale, FL, March 16-19, 2009.
- [7] National Renewable Energy Laboratory, *Design of Electric Drive Vehicle Batteries for Long Life and Low Cost*, Golden, CO, 2010, NREL/PR-540-48933.
- [8] Idaho National Laboratory, *Technology Life Verification Testing*, Idaho Falls, ID, 2010, INEEL-EXT-04-01986.
- [9] J. Wang, P. Liu, J. Hicks-Garner, E. Sherman, S. Soukiazian, M. Verbrugge, H. Tataria, J. Musser, P. Finamore, "Cycle-life model for graphite-LiFePO₄ cells," *J. Power Sources* 196(2011) 3942-3948.
- [10] S. Peterson, J. Apt, J. Whitacre (2010) "Lithium-ion battery cell degradation resulting from realistic vehicle and vehicle-to-grid utilization," *J. of Power Sources*, v195 p2385-2392.
- [11] S. Santhanagopalan, Q. Zhang, K. Kumaresan, R.E. White, "Parameter estimation and life modeling of lithium-ion cells," *J. Electrochem. Soc.* 155(4) 2008, A345-A353.
- [12] M.W. Verbrugge, Y.-T. Cheng, "Stress and strain-energy distributions within diffusion-controlled insertion-electrode particles subjected to periodic potential excitations," *J. Electrochem. Society*, 156(11) 2009, A927-A937.
- [13] M. Broussely, "Aging of Li-ion batteries and life prediction, an update," 3rd Int. Symposium on Large Lithium-Ion Battery Technology and Application, Long Beach, California, May 2007.
- [14] J. Hall, T. Lin, G. Brown, P. Biensan, F. Bonhomme, "Decay processes and life predictions for lithium ion satellite cells," 4th Int. Energy Conversion Engineering Conf., San Diego, California, June 2006.
- [15] M. Smart, K. Chin, K., L. Whitcanack, B. Ratnakumar, "Storage characteristics of Li-ion batteries," NASA Battery Workshop, Huntsville, Alabama, Nov. 2006.
- [16] M. Broussely, Chap. 13 in: *Advances in Lithium-Ion Batteries*, van Schalkwijk, W., and Scrosati, B., editors. New York: Kluwer Academic / Plenum Publishers, 2002.
- [17] M. Ojah, D. Pearson, "2006 Austin/San Antonio GPS-Enhanced Household Travel Survey," Texas Transportation Institute, August 2008.
- [18] M. Earleywine, J. Gonder, T. Markel, M. Thornton, "Simulated fuel economy and performance of advanced hybrid electric and plug-in hybrid electric vehicles using in-use travel profiles," Vehicle Power and Propulsion Conference, Lille, France, Sept. 2010.
- [19] U.S. Department of Transportation, Federal Highway Administration, 2005 National Household Travel Survey. URL: <http://nhts.orl.gov>.
- [20] E. Wood, J. Neubauer, J. Gonder, A.D. Brooker, K. Smith, "Variability of battery wear in light duty plug-in electric vehicles subject to ambient temperature, vehicle design and consumer usage," submitted to 26th Int. Electric Vehicle Symposium, Los Angeles, CA, May 6-9, 2012.
- [21] K. Smith, M. Earleywine, E. Wood, J. Neubauer, A. Pesaran, "Comparison of plug-in hybrid electric vehicle battery life across geographies and drive cycles," SAE World Congress, Detroit, MI, April 24-26, 2012.